Investigation of Electrospray Ionization and Electrostatic Focusing Devices Using a Three-Dimensional Electrospray Current Density Profiler

J. Will Thompson, John W. Eschelbach, Richard T. Wilburn, and James W. Jorgenson
Department of Chemistry, University of North Carolina, Chapel Hill, North Carolina, USA

A novel instrument for profiling the current density of nanoelectrospray ionization plumes in three dimensions has been developed. A hemispherically-shaped electrostatic lens at atmospheric pressure is found to be able to compress the space-charge in nano-ESI and increase the average current density in the plume to three times the nominal value. Ion transmission into a single-quadrupole mass spectrometer is found to roughly double using the electrostatic lens. Data also suggest that ion transmission into the first vacuum region for a skimmer-type mass spectrometer interface using nano-ESI may be typically 40% or better with no special focusing device used. (J Am Soc Mass Spectrom 2005, 16, 312–323) © 2004 American Society for Mass Spectrometry

Since its inception as an ionization technique for mass spectrometry in 1984 [1], electrospray has enjoyed an explosion in use. Two factors have emerged that determine sensitivity for an analyte in electrospray ionization mass spectrometry (ESI-MS): ionization efficiency and ion transfer efficiency [2–6]. Ionization efficiency is the fraction of target molecules in the liquid phase that evolve into gas phase ions via the ESI mechanism. ESI inherently has high ionization efficiencies due to the large number of excess charges available for protonating or deprotonating analyte molecules (positive and negative modes, respectively) [2, 7]. The advent of nanoelectrospray (nano-ESI) further benefited ionization efficiency because lower flow rates lead to smaller initial droplet size and larger amounts of excess charge per unit volume. It is widely accepted that nano-ESI exhibits superior ionization efficiency over conventional ESI or ionspray techniques, and efficiencies at very low flow rates are thought to approach 100% [8–12].

Ion transmission efficiency is the fraction of analyte ions that enter the mass analyzer out of those gas-phase ions produced, and is largely a characteristic of the mass spectrometer. The number of analyte ions that are transferred from one region to the next is proportional to the current density (J) at the entrance orifice of the mass spectrometer and the gas flow into the MS at that orifice [13]. Since ESI is typically performed at atmospheric pressure, the efficient transfer of gas phase ions from ambient pressure to high vacuum required for mass spectrometry was recognized as an important sensitivity issue during the technique's infancy [14, 15]. Due to the coulombically repulsive nature of an ESI plume and the characteristic losses of skimmer devices, ion transmission from source to detector in ESI-MS has been quoted as being as low as 1 ion transmitted in 10^5 ions created [2, 16]. The largest losses appear to occur between the ESI source and the first sampling orifice. Current measurements behind the first sampling orifice have historically been about two orders of magnitude smaller than the total ESI current, indicating about one percent ion transmission into the first differentially pumped region [10, 16–18].

One attempt to improve transmission between the electrospray source and first sampling orifice included enlarging the entrance orifice and using a higher pumping speed [19, 20]. Although this method is effective, larger pumps are needed, which can lead to prohibitive costs. A thoroughly studied method for improving ion transmission in ESI-MS is the so-called "Ion Funnel", which was based on early work by Bahr et al. and developed in the laboratory of Richard Smith [18, 19, 21–28]. This device showed improvement in ion transmission into the mass analyzer, but was not functional at atmospheric pressure. Lee and coworkers have recently shown transmission improvements using a Venturi device, in an approach based on gas dynamic focusing [29]. Perhaps the method of increasing ion transmission that has received the most coverage in the literature is the use of electrostatic lenses, but signal

Published online January 14, 2005
Address reprint requests to Dr. J. W. Jorgenson, Department of Chemistry, University of North Carolina at Chapel Hill, CB 3290, Venable Hall, Chapel Hill, NC 27599-3290, USA. E-mail: jj@unc.edu

1044-0305/05/$30.00
doi:10.1016/j.jasms.2004.11.012

Received July 12, 2004
Revised November 17, 2004
Accepted November 17, 2004

improvements and exact function or benefit of these methods has not been well established [14, 15, 30–33].

More recently, Schneider and coworkers used an "atmospheric pressure ion lens" in the form of a ring to improve ion transmission by shaping the electric field between the ESI emitter and acceptance orifice [34]. Previously, Beavis et al. used a similar device to assist in electrospray deposition of LC eluate into a small spot for off-column analysis by SIMS [35, 36]. Our study will focus on the evaluation of these types of electrostatic devices. We have also adopted the terminology "ion lens" to include the use of electrostatic fields to move ions at atmospheric pressure. Previous works have evaluated electrostatic lens effects on ESI strictly on the basis of how transmission of ions into a mass spectrometer is altered; in other words, the ion signal has been the primary quantity measured. Our investigation centers around profiling the effect of electrostatic lenses on the actual shape and current density of the electrospray plume, in addition to directly monitoring the resultant ion transmission into a mass spectrometer.

The ESI profiler described herein allows complete three-dimensional generation of current density profiles for nano-ESI plumes. Visualization of electrospray plume geometry is commonly performed using photomicroscopy. The main weakness of this technique is that once the electrosprayed droplets become too small to scatter light, the spray plume is not visible. In our experience with nano-ESI techniques, this can occur within one millimeter or less of the spray tip. Zhou and coworkers have used fluorescence techniques to monitor ion intensity as a function of location in an ESI plume, and more recently to monitor pH changes that occur in the plume [37, 38]. Although this technique provided the first direct measurement of ion intensities in an ESI plume, the spatial resolution was limited to 1 mm. By monitoring the local current density with a very small probe electrode, our ESI profiler can detect current density changes with a resolution of roughly 0.5 mm. Simultaneous monitoring of the total ESI current from the ground plane ensures consistent ESI performance over time. This is important because an accurate ESI profile can only be accomplished with the plume at a steady spray state.

To our knowledge, this report contains the first generation of complete geometric current density profiles for electrospray ionization. A goal of this study is to show how electrostatic lenses at a voltage between that of the emitter and electrical ground affect the shape of nanoelectrospray plumes. In addition, the current transmitted into the orifice of a mass spectrometer can be increased by using such an electrostatic lens. A simple way to address the increase in ion signal due to compression of the space charge is developed as a term designated "compression factor", or κ. This term is developed as a ratio of the average current densities of electrospray plumes before and after focusing with electrostatic lenses.

Experimental

Electrospray Profiler

An instrument to profile the current density of an electrospray ionization plume in three dimensions was fabricated from parts both ordered and machined in-house. All materials were obtained from McMaster-Carr Supply Company (Atlanta, GA) unless otherwise noted. A simplified schematic of the assembled ESI profiler is shown in Figure 1. The general experimental design involves using a brass plate (15.25 cm square $\times$ 0.635 cm thick) at ground potential as the ground plane for electrospray ionization. The plate has a 1 mm hole drilled into the center, through which a 500 μm-diameter copper probe electrode is placed (PE in Figure 1), such that the electrode is exactly level with the brass ground plate surrounding it. The probe electrode was fabricated by using heat-shrink tubing to surround a piece of 500 μm copper wire (total diameter 1 mm), after which the insulated wire was clipped and polished using 2000-grit sandpaper followed by 0.5 μm diamond compound (Crystalite Corp., Marina del Rey, CA). The nonpolished end was soldered to a low-noise BNC cable. This small electrode was used to monitor current density as a function of position within the electrospray plume. Another low-noise BNC cable was connected directly to the brass plate to monitor total electrospray current (labeled I_T in Figure 1).

Current from the 500 μm probe electrode was amplified by 10^8 to 10^9 volts/amp using a Keithley model 427 current amplifier (Cleveland, OH) and subsequently recorded with a Dell Dimension XPS T700R personal computer (Round Rock, TX), using a BNC-2090 break-out box (National Instruments Corporation, Austin, TX). Total electrospray current was monitored using a Keithley model 616 digital electrometer (Cleveland, OH).

The probe electrode and ground plate assembly were attached to a moving stage using 7.6 cm-long 3/8–16 stainless steel bolts. These bolts were run through a 0.635 cm polycarbonate plate to provide electrical isolation. The polycarbonate plate was then bolted to a low-profile Teflon guide block that fit into a 75 mm-wide $\times$ 500 mm-long aluminum rail for y-translational movement (labeled "Y" in Figure 1). Another polycarbonate block (1.27 cm thick) was used to couple the y-translational rail to a Versa-Mount ball-bearing guide block for x-translation. This guide block fit around a 45.7 cm-long hardened steel guide rail (labeled "X" in Figure 1). The entire assembly was bolted to a laser table (Technical Manufacturing Corporation, Peabody, MA).

Translation was accomplished in the X and Y directions using linear actuators. Actuators (model 36341-05-061, Haydon Switch and Instrument, Inc., Waterbury, CN) were attached via aluminum angle brackets to the X and Y translational stages, as shown in Figure 1 (X-dimension motor and lead screw not shown). The linear actuators were operated by microcontroller-

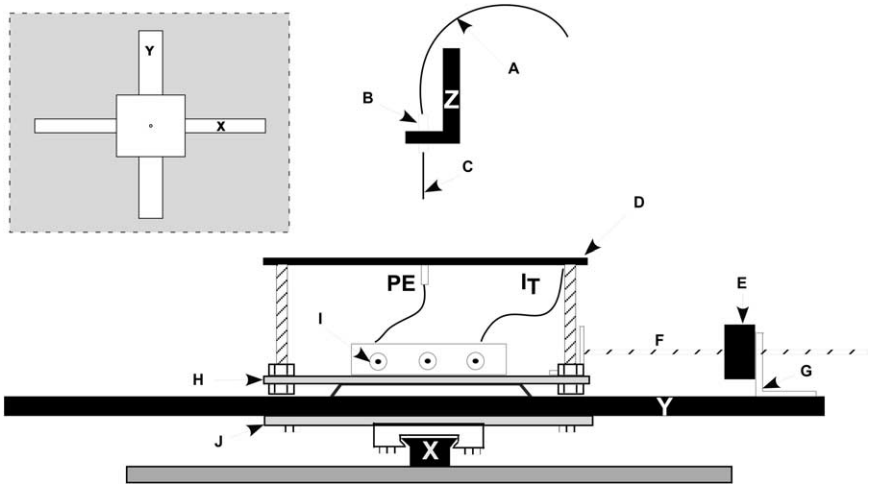

Figure 1. Schematic of electrospray current density profiler, side view. (A) Fused silica infusion capillary. (B) Teflon butt-connect. (C) Electrospray needle. (D) Brass ground plane. (E) Linear actuator for Y-translation. (F) Lead screw for Y-translation. (G) Aluminum bracket. (H) Polycarbonate insulator between ground plane and Y-translation stage. (I) BNC connectors. (I_T) Lead to monitor total ESI current. (J) Polycarbonate insulator between X- and Y- translational stages. (PE) Probe Electrode. (X) X-translation track. (Y) Y-translation track. (Z) Z-translation micropositioner. Inset: Top-down layout of ESI profiler. Linear actuator and lead screw for X-translation not shown.

based stepper motor control boards. The main control board consisted of a BiStep A06 (Peter Norberg Consulting, Inc., Ferguson, MO) operated in 1/16th microstepping mode to produce smooth linear motion and increased resolution. The control board was interfaced to a custom data acquisition and motion control program written in LabView 6.1 (National Instruments Corporation, Austin, TX). Positional information of the probe on the X- and Y-axes was calculated from the step number of the linear actuator provided by the stepper control board.

Electrospray ionization was performed via infusion using platinum-coated fused silica Picotips (model FS360-20-5-D and FS360-50-8-D, New Objective, Inc., Woburn, MA) butt-connected to fused-silica tubing with Teflon® tubing (Polymicro Technologies, LLC., Phoenix, AZ). A pressure bomb was used to supply liquid flow and a 5 kV DC power supply (Bertan model MPS-HV10M-05P, Valhalla, NY) was used to couple the spray voltage directly to the spray tip. The electrospray emitter was positioned vertically, spraying down on the profiling apparatus (see Figure 1). Fine control of the vertical position ("Z-dimension") of the spray tip was performed utilizing a micropositioner with 0.01 mm precision, (Narishige Intl., Tokyo, Japan) fitted with an in-house machined polycarbonate bracket to couple the positioner to the butt-connect (Z in Figure 1). The micropositioner was bolted to a square polycarbonate stage which was fabricated in-house, having legs approximately 30 cm long that were bolted to the laser table to provide positional stability of the electrospray needle.

Lenses

Electrostatic lenses were machined out of either stainless steel or brass from 3/4-inch round stock. Several lenses were tested, including ring, conical, and hemispherical designs. This paper will focus on the properties of one lens design, the inverted hemispherical lens. For this lens, round brass stock was machined to 19.0 mm diameter and 10.6 mm length. A 16 mm ball endmill was used to cut a hemisphere to 9 mm depth. Then a 3.1 mm hole was drilled axially for the insertion of the ESI needle. Figure 2 shows the normal orientation

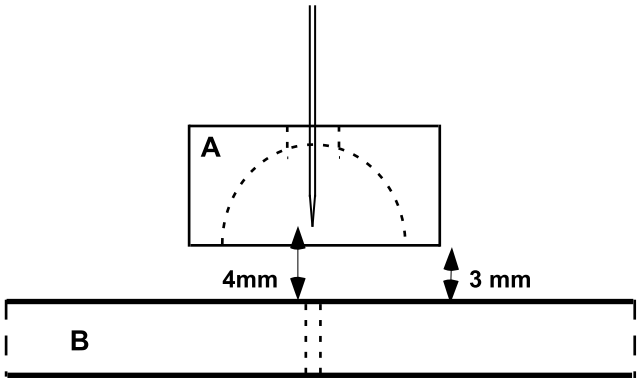

Figure 2. Orientation of hemispherically shaped electrostatic ion lens. (A) Ion lens in inverted orientation found to be most functional for focusing ESI plume at atmospheric pressure. Lens machined of brass. Dimensions given in Experimental section. (B) Ground plane of electrospray current density profiler. Drawing shows the most effective lens geometry in relation to the ESI needle, with the needle 1 mm within the exit of the lens. Drawing not to scale.

of this lens in relation to a spray needle and the ground plane of the ESI profiler. To hold the lenses in place, a model RSA-1 rotating optical positioner (NRC, Fountain Valley, CA) was fitted with a specially made aluminum bracket that allowed positional adjustment relative to the electrospray needle. The base of the rotating optical positioner was bolted on the underside of the polycarbonate stage (also used to hold the Z-positioner). This assembly allowed for quick insertion of the lens to a reproducible location. A separate output of the 5 kV DC power supply described above provided the lens voltage.

Chemicals

HPLC-grade acetonitrile, HPLC-grade methanol (Fisher Scientific, Fair Lawn, NJ), formic acid, 96% (Aldrich, St. Louis, MO), and ammonium bicarbonate (Sigma Chemical Co., St. Louis, MO) were used as received. Water used in these experiments was purified (18 MΩ*cm) using a Nanopure ultrapurified water system (Barnstead International, Boston, MA). All solutions were filtered through 0.1 μm nylon syringe filters prior to use (Cameo 30N Syringe Filter, GE Osmonics, Inc., Trevose, PA).

Collecting an Electrospray Current Density Profile

To collect a profile, the ESI needle was first set at the desired distance from the ground plane ("Z"-distance). The brass plate was then translated under the electrospray plume so that the probe electrode traversed a square area in a flat s-fashion. This process was carried out in the following steps: the probe electrode was positioned in the left, lower corner of the plane to be profiled, and then scanned from left to right (+X direction). Next, the probe electrode was moved closer to the center of the ESI plume in a Y-step of previously determined distance. The probe was then scanned back from right to left (−X direction), followed by another Y-step. This process was repeated until the desired area was covered. Data was collected at 20 Hz only during the ±X-directional scans, and each line scan was saved to an individual file. The typical rate of translation was 0.05 inches (0.13 cm) per second. For normal operation, a survey scan with a Y-step of 1 mm was often used to make sure the profiled area captured the entire electrospray plume. The survey scan typically took less than 2 min. Provided the profiled area did not need to be adjusted, this could then be followed with a scan at high resolution, which typically utilized a 0.250 mm Y-step. A 10 mm × 10 mm scan at this resolution could be performed in about 7 min. The maximum reproducible position in the Y-direction for this instrument is roughly 0.05 mm. For profiles taken at high resolution (Y-step less than 1 mm), only the +X-directional scans were used, in order to eliminate the mechanical actuator hysteresis of about 100 μm.

Data Manipulation

Individual data files for each scan were typically combined in a Labview program to form a slice plane, and subsequently loaded into Igor Pro 4.08 for visualization (Wavemetrics, Inc., Oswego, OR). To improve visual display of data collected from the profiler, a 200 × 200 point grid interpolation was often performed using Igor Pro. Scans could be loaded individually in cases where comparison of electrospray plumes under multiple conditions was needed; in this case the most intense line scan in the two dimensional profile was selected and then plotted as current density versus X-translational distance. Three dimensional volume visualization and data manipulation was performed using a custom module written in AVS/Express (Advanced Visual Systems Inc., Waltham, MA). The volume was created by first stacking multiple slice planes along the Z-axis and then performing a first-order, nearest-neighbor interpolation into a regular grid. The interpolated grid was equal to or less than the dimensions of the irregularly sampled input grid to produce the most accurate image.

Direct Measurement of Ion Transmission

Ion transmission through the acceptance orifice of a mass spectrometer was determined by ratioing the current measured at a small Faraday mesh detector immediately behind the entrance orifice to the total current of the nanospray plume. All MS experiments were performed on a Waters Micromass ZQ single quadrupole mass spectrometer (Waters Corporation, Milford, MA). The orifice diameter on this instrument was 500 μm. The ion block portion of the ZQ was modified to allow a stainless steel mesh electrode to be suspended in the ion flow path at a distance of 17 mm behind the orifice to measure the ion current transmitted through the acceptance orifice. Pressure in this region was approximately 3 torr. The mesh used was woven from 50 μm fibers and had approximately 40% open area; this was cut into a 5 mm circle and subsequently soldered to 22 AWG Duobond shielded 50 ohm coax cable (Belden Wire and Cable, Richmond, IN). The mesh electrode current was monitored using a Keithley model 616 digital electrometer (Cleveland, OH). At a bias voltage of 50 V between the surrounding ion block and the mesh electrode, the collection efficiency was calculated to be 96%. It is important to mention that current measurements behind the first orifice can only approximate the increase in signal that may be seen after at the mass analyzer; there are effects such as ion beam shape and gas dynamics in the interior of the MS that are not taken into account by our experiments. In addition, the mesh electrode collects the current transmitted; it is not selective between gas-phase ions, ions that are still partially solvated, or even charged droplets.

Infusion nano-ESI and capillary liquid chromatography ESI-MS experiments were performed to evaluate

lens performance. Nano-ESI was performed on-axis with the acceptance orifice since the electrostatic lens focuses the plume in an axial direction. A Waters Nanospray source was used to hold the electrostatic lens and a second micropositioner was used to hold the nanospray needle. The total electrospray current was monitored by using a multimeter floated at high voltage to track the voltage drop across a 4.13 MΩ carbon resistor in series with the applied spray voltage.

Evaluation of Percent Coverage in Protein Digest Experiments

A capillary column (30 μm i.d. fused silica, Polymicro Technologies, Phoenix, AZ) was slurry packed in house to a length of 50 cm with Atlantis 3 μm C18 porous silica particles (Waters Corporation, Milford, MA), using a packing apparatus previously reported [39]. Separations of a tryptic digest of bovine serum albumin (MassPREP BSA Digestion Standard, Waters Corporation, Milford, MA) were performed and percent coverage was determined using selected ion searching over the mass range of 400 to 1500 *m/z* (Biolynx and Masslynx mass spectrometry software, Waters Corporation, Milford, MA). Injections from approximately 600 amol to 200 fmol protein digest were performed using a pressure bomb and varying dilutions. Percent coverage was compared head-to-head for using the hemispherical lens versus not using the lens, operating with the spray needle in the same position (4 mm from sampling orifice).

Theory

Electric Field

The electric field (E) at an electrospray tip can be calculated using the equation:

$$E = \frac{V}{A \cdot r \cdot \ln\left(\frac{4d}{r}\right)} \quad (1)$$

where V is the applied voltage, r is the capillary emitter radius in cm, and d is the distance between the ESI tip and the ground plane in cm [40, 41]. A is an empirical constant found by Smith to be equal to 0.667 [41]. It is important to note that eq 1 was derived for the electric field at a point relative to a plane, and thus cannot be used to calculate the field at an electrospray tip in the case where an electrostatic lens is in place.

Current Density

ESI profiles obtained with our system generate two current measurements. The first current measurement comes from the probe electrode, PE, which provides a current density at a specific location in the electrospray plume, defined as current per unit area, J:

$$J = \frac{i_p}{A_p} \quad (2)$$

where i_p is current in amperes at the probe electrode and A_p is probe electrode area in mm^2. Local current density (J) was plotted in our experiments to show changes in the intensity of the electrospray plume as a function of position.

The other current measurement obtained in these experiments is total electrospray current (I_T), in amperes, which should be constant throughout a profiling run for constant ESI conditions. Using this measured current, an average current density for an electrospray plume, or $\bar{J}$, can be described as

$$\bar{J} = \frac{I_T}{A_T} \quad (3)$$

where A_T is the total area in mm^2 that the electrospray plume covers at the brass ground plane, obtained for each case from the ESI profiler data. Average current density can therefore be defined for an electrospray plume under any number of varying conditions such as spray voltage, solvent flow rate, emitter-ground plane distance, or various lens parameters.

Compression Factor

Electrostatic lenses, gas dynamics, and other means have been used in attempts to increase ion transmission from ESI into the mass spectrometer, as outlined in the introduction. A general difficulty in reviewing the literature is that there has been no uniform way to determine the effectiveness of the various techniques at shaping the electrospray plume and getting more ions into the entrance orifice. Improvement in terms of limits of detection always depends on the starting conditions which the experimenter chose and the MS instrument employed. To more accurately compare effectiveness of focusing methods on ESI plumes, the simple concept of compression factor has been developed. Compression factor, or κ, can be described as

$$\kappa = \frac{(\bar{J}_L)}{(\bar{J}_N)} \quad (4)$$

where $\bar{J}_L$ is the average current density (A/mm^2) for the lens condition, and $\bar{J}_N$ is the average current density under nominal or unmodified conditions. The ratio κ essentially provides a value for the compression of the space-charge in an electrospray plume, as compared to the null condition. A $\kappa > 1$ can manifest itself in an electrospray profile as an increase in current density, J, in the central portion of the profile. If the entrance orifice of a mass spectrometer is a fixed diameter, compression of the ion current into a smaller area in front of the orifice should allow for increased ion

transmission, assuming the orifice diameter is smaller than the plume diameter. The parameter κ is normalized by the nominal case for any particular system, and thus eliminates other instrumental variables such as flow rate, spray voltage, and solvent viscosity in determining the focusing effectiveness of any focusing system.

Results and Discussion

Operation of the Nanoelectrospray Profiler

The technique used for collection of a nano-ESI current density profile was described in the experimental section. Important to the function of this device is that the translation of the brass ground plane is "invisible" to the electrospray emitter; this ensures that the electric field does not change over the course of stage translation and an accurate profile is generated. The ground plane area in this system is large enough that the emitter never approaches the edge of the brass plate, so the distance relevant to the formation of the electric field between emitter and ground [41] remains constant throughout X-Y translation. Total electrospray current is monitored at all times to ensure consistency in the electrospray mode.

Current Density as a Function of Distance from the ESI Emitter

Current density profiles were collected as a function of distance from the ESI needle. A New Objective picotip with 8 μm orifice diameter was used to spray a solution of 50/50 acetonitrile/water with 0.1% formic acid at 150 nL/min. Current density profiles were collected at 1 mm increments from 2 to 12 mm from the ESI needle, then stacked in Z-space to create a three-dimensional current density map. An important property of this experiment was that as distance was increased, the voltage applied to the ESI needle was increased to maintain a constant electric field at the ESI tip of roughly 1.1×10^6 V/cm as calculated using eq 1. This was confirmed also by consistent I_T during all measurements. It was expected that we would observe a widening spray plume as distance from the needle increased, due to the diverging electric field lines near the emitter and coulombic repulsion of the ions in the plume [13, 40, 41].

In 1991, Busman et al. published finite element calculations for the charge density as a function of distance from an electrospray emitter based on a "needle-in-can" geometry [13]. Figure 3a shows a contour plot of the calculated charge density, based on a hypothetical source with radius 1cm at 5 kV and a ground plane at a distance of 5 cm. Figure 3b is a contour plot of current density as a function of distance taken using our ESI profiler. Both the mathematical model and our experimental data point to a collimated spray plume close to the emitter where the ions are in a strong electric field. Then, after the field strength lessens, the plume diverges significantly into more of a mushroom shape. Our experiments reinforce Busman's model that the ions spread more readily in a space-charge dominated region far from the emitter, however it is possible this may be partly due to increased ion mobility as desolvation of the ions occurs. In the Busman model, the expansion was attributed totally to field strength, and ion mobility was held constant. The absolute values of current and charge density, distance, spray voltage and electric field were different for the experimental and calculated systems. Nonetheless, it is noteworthy that there is such strong agreement in the geometry that ions undergoing coulombic repulsion during ESI seem to obey in Busman's model and in our experiments.

Neither our experiments nor the Busman model include the effects a gas-dynamic acceptance orifice to a mass spectrometer may have on the electrospray plume. The high-velocity gas flow into the acceptance orifice certainly serves to increase the number of ions transmitted, and may change the shape of the ESI plume at small distances from the orifice.

Recognition of Spray Tip Integrity

An immediate benefit of the ESI current density profiler was the instrument's ability to recognize nanoelectrospray needles that were in poor condition. Figure 4 is a comparison of an ESI profile for a needle in poor condition (4A) and a new needle (4B). This experiment was performed over a 20 mm $\times$ 20 mm area with a Y-step of 1 mm. Both profiles were taken at a distance of 12 mm from the spray tip, with a spray voltage of 3.06 kV, a volumetric flow rate of roughly 200 nL/min (50/50 ACN/H_2O with 20 mM ammonium bicarbonate). Figure 4a shows an ESI profile that was taken using a fused silica needle which was pulled with an electric arcer and etched in-house to make a tip with inner diameter roughly 5 μm. This needle had a small chip at the end, which was observed upon microscopic evaluation. Figure 4b was obtained using a new FS360-50-8-N fused silica tip from New Objective. There were multiple jets emitting from the spray tip; in particular, a major jet in the 6 mm region on the y-axis, and a minor jet near 14 mm, as annotated in Figure 4a. Profiles were taken over a wide range of spray voltages to ensure these multiple spray jets were not due to operating outside the most stable cone-jet mode.

Recommendations have been made in the literature for cleaning or unclogging nano-ESI needles by carefully scratching them on the surface of a ground plate [10]. Evidence presented in Figure 4 suggests that jagged nano-ESI emitters, as may be produced by them touching a surface, give less than desirable electrospray plume characteristics. In general, our evaluation of several in-house made electrospray needles showed that they gave less reproducible and less uniform spray characteristics than the New Objective needles. There-

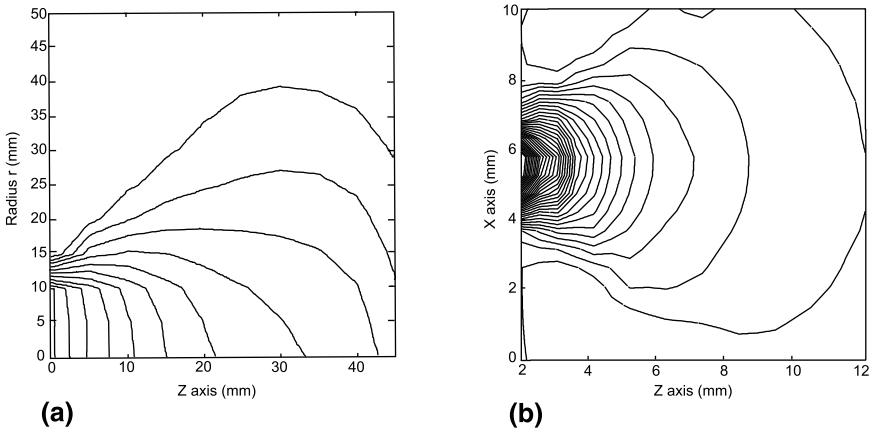

Figure 3. Ion density as a function of position within an electrospray plume. (**a**) Finite-element calculations for needle-in-can geometry. Charge density distribution (-10^{-5} C/mm^3 per step) where the needle is located at (0 meters Z, 0 through 0.01 meters r). Reprinted from reference [13] with permission of Jan Sunner (author) and Elsevier Publishing. (**b**) Interpolated current density distribution (-1.53 nA/mm^2 per step) where needle is at position (0 mm Z, 4.7 mm X). Electrospray was performed with the electric field at the tip constant at approximately 1.1×10^6 V/cm. Flow rate was 150 nL/min of 50/50 water/acetonitrile with 0.1% formic acid.

fore, the commercially made needles were used for all other experiments and the needle was replaced any time there was a chance it had become damaged.

Observation of Multiple Spray Modes Using an Electrostatic Lens

Several different lens designs were tested in our experiments, including ring electrodes and different interior diameters of conical and hemispherical shape. In all cases, the lens orientation was similar to that used by Schneider et al., although that report only contained data for a ring-like electrostatic lens [34]. Figure 2c shows the lens arrangement using a lens with a hemispherical interior, with a 3.1 mm hole in the top where the spray needle protrudes. When a lens with this shape was modeled using Simion 7.0, the resulting electric field at the spray tip had isopotential lines that were somewhat flattened as compared to a model where no lens was used (data not shown). Supporting this modeled system, we observed two regions of steady decrease in total ion current (I_T); from 0 to 600 V (V_L) and from 650 to 1300 V (Figure 5a). These regions also had linear increases in current density at the center of the ESI plume (Figure 5b). This suggests the electric field at the tip is being modified and that coulombic repulsions are being counteracted by the additional electric field from the lens.

The two sudden drops in spray current near V_L = 600 and 1350 V correspond to changes in the axial spray

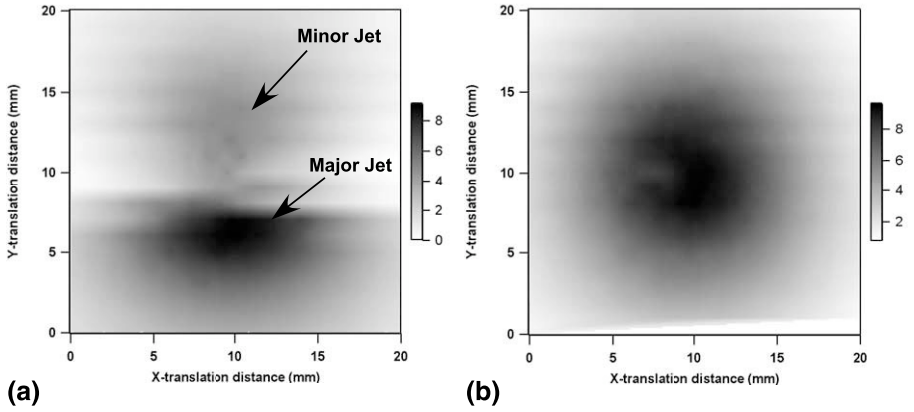

Figure 4. Profiles of electrospray plumes with electrospray needle in poor condition (**a**) and with a new New Objective FS360-50-8-D needle (**b**). Data was interpolated into a 200 × 200 grid using Igor Pro 4.08. Needle to plane distance = 10 mm; spray voltage = 3.02 kV; flow rate was roughly 200 nL/min of 50/50 water/acetonitrile with 0.1% formic acid. Collection was over a 20 × 20 mm square with Y-resolution of 1 mm. The grayscale legend to the right of the plots gives current density (J) in nA/mm^2.

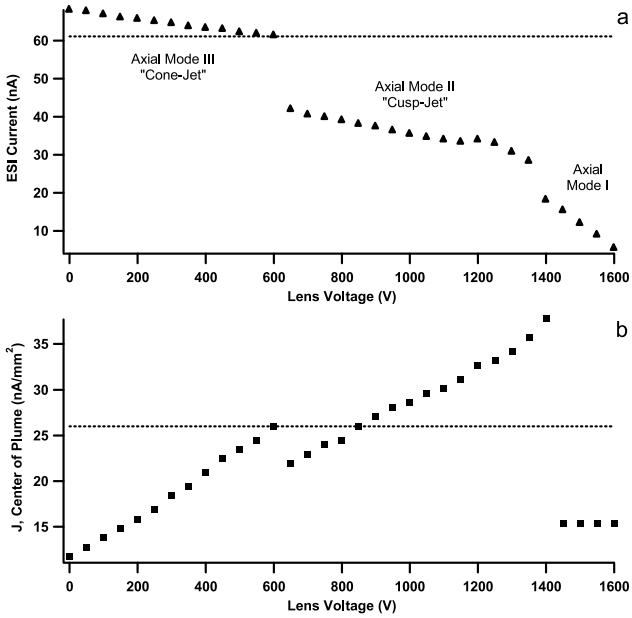

Figure 5. Current as a function of lens voltage with constant ESI voltage. Data parameters: F = 15 nL/min; 90%/10% water/acetonitrile with 0.1% formic acid; ESI voltage 1.6 kV. Needle and lens setup as shown in Figure 2. (**a**) Total ESI Current as a function of lens voltage. (**b**) Current Density (J) in the center of the ESI plume as a function of lens voltage (monitored at the 0.5 mm probe electrode). Dotted lines correspond to the nominal case, or the values of total current and current density with no lens in place.

mode. Our observations correlate well with the three axial spray modes reported by Juraschek and Röllgen [42]. At high V_L there were heavy pulsations in I_T, corresponding to axial spray mode I, which occurs at low spray potentials. The region between V_L = 650 and 1350 V corresponds to axial spray mode II, or "cusp-jet" mode, and the highest current region corresponds to the preferred "cone-jet" mode, or axial spray mode III, as labeled in Figure 5. An initially surprising result was that I_T was higher with the lens in place and V_L less than 600 V, than with no lens present at all. The horizontal dotted line in Figure 5a at 61 nA corresponds to the nominal I_T for this system with no lens in place. Having a lens at low potential near the ESI needle raises the electric field and therefore raises I_T. Total spray current returns to its nominal value of 61 nA when V_L reaches 600 V. This data suggests that the lens is located at a position where the usual potential in space, with V_s = 1600 V, would be roughly 600 V.

Spray modes II and III appear to be effectively focused by the electrostatic lens, as is evident in Figure 5b by the linear increase in current density at the center of the plume during both modes. Here again, the dotted line indicates the nominal value of J, or the value of current density in the center of the ESI plume with no lens being used. J values lower than the nominal case mean that the ESI plume is being widened by the lens because the ions are attracted to the low potential lens. Therefore, no actual compression of the ESI plume occurs in the cone-jet spray mode as compared to the nominal case. Local current density (J) at the center of the plume can be roughly doubled while maintaining constant V_s, but the plume is operating in the less desirable cusp-jet mode and I_T is significantly diminished.

Total current of an electrospray plume has been studied as a function of a number of parameters, including but probably not limited to, solvent flow rate, spray voltage, emitter-ground plane distance, solvent conductivity, emitter diameter, and solvent viscosity [2, 3, 5–7, 12, 17, 41, 43–46]. The total spray current is directly proportional to the amount of excess charge available to produce gas-phase ions [47, 48]. In all of our other experiments utilizing electrostatic lenses, V_s was adjusted as V_L was increased in order to maintain constant total ESI current and keep the electrospray in the desirable cone-jet mode.

Profiling Local Current Density Enhancement Using Electrostatic Lenses

A significant conclusion of the previously mentioned Busman et al. model was the prediction that no improvement in current density, and thus MS signal, could be obtained by using electrostatic lenses [13]. The model, however, used as the focusing case a situation where the lens was at the same potential as the emitter. This is an unrealistic configuration for ESI because the field is so weak at the ESI tip that no Taylor cone can form, and therefore no emission will occur. The analogous case in our data is shown in Figure 5a where V_L is 1600 V. Compression of space-charge in ESI to increase current density at the orifice of a mass spectrometer can be carried out via electrostatic lenses, but it must be done in a situation where the strong electric field at the ESI tip is maintained and the total spray current is constant. This requires increasing the spray voltage as the surrounding electrostatic lens voltage is increased.

The electrospray profiler was used to image changes in current density that occurred when the voltage was increased on an electrostatic lens positioned as in Figure 2. V_s was adjusted to maintain constant I_T. Figure 6 is a plot of local current density, J, versus position as the probe electrode was traversed along the X-axis, for four different V_L values. The exact collection parameters are included in the caption for Figure 6. In comparison to the nominal case (Figure 6, Trace A), the ESI plume was noticeably widened when the lens was at ground potential, and the local current density in the center of the plume was cut in half (Figure 6, Trace B). It is expected that a broadened plume would lead to a decrease in ion transmission efficiency. This occurs because the ions are attracted to the electrostatic lens acting as a ground plane.

At V_L = 400 V, the ESI plume shape is almost identical to the plume where no lens is present (data not

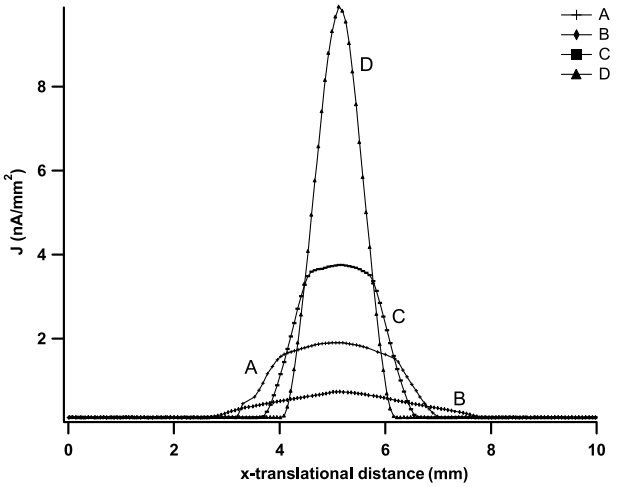

Figure 6. Effect of a hemispherical lens on current density profiles of an ESI plume. Plotted are the most intense (central) scans for each of four different conditions. All scans collected with 40% acetonitrile in 0.1% formic acid; F ~ 15 nL/min; I_T was constant at 36 nA; needle and lens orientation is as shown in Figure 2. (**a**) V_S = 1600 V, no lens used. (**b**) V_s = 1550 V, V_L = 0 V. (**c**) V_s = 1850 V, V_L = 800 V. (**d**) V_s = 2680 V, V_L = 2000 V.

shown). Further enhancement of the current density in the center of the plume is noticeable as V_L is raised to 800 and 2000 V (Figure 6, Traces C and D, respectively). Current density values in the center of the plume were increased approximately from 2 nA/mm^2 in Case A to 10 nA/mm^2 in Case D. If ion transmission were only dependent upon this local J, the increase observed in Figure 6a to d would correspond to an approximately 5-fold increase in signal.

Increases in Average Current Density and Compression Factor Using Electrostatic Lenses

The orifice of a mass spectrometer functions not as a point, but as an active gas dynamic region. It has a functional diameter that is larger than the actual diameter itself, due to the high gas flow into the orifice. Ion transmission can therefore be better approximated by the average current density ($\bar{J}$) of an ESI plume in the region sampled by the entrance orifice [13]. Figure 7a shows the increase in average current density as a function of lens voltage for three different mobile phase compositions. It is immediately noticeable in Figure 7a that the mobile phases with higher aqueous content, and thus higher conductivity, exhibit higher overall $\bar{J}$ values, which is concurrent with literature [12, 37, 46]. In addition, the slope of $\bar{J}$ versus V_L also decreases with increasing organic content (i to iii). This would prematurely suggest that higher organic content plumes are less effectively focused using atmospheric pressure lenses.

However, if compression factor (κ) is calculated for the same system, a different trend is observed. This factor takes into account the current density of the nominal, or unfocused, case. A κ value of 1 indicates $\bar{J}$ is the same as that of the nominal case, and should correlate to the same ion transmission as in the nominal case. Figure 7b shows that for V_L = 2000 V, κ is roughly 3, predicting a 3-fold increase in ion transmission over using no lens. For Figure 7b, it is also important to note that the slopes of all κ versus V_L curves are nearly the same, indicating that the lens affects the spray plume the similarly for all organic solvent compositions. In fact, the absolute values for κ are slightly higher for high organic content under all lens voltages, suggesting that an ESI plume with high organic content may in fact be easier to focus. In a separate experiment, we observed the same optimal V_L conditions for mobile phases of 5 to 80% acetonitrile composition. Lens voltage should not have to be adjusted to maintain high ion transmission efficiencies during a gradient liquid chromatography run, for instance.

It is also of interest to note that we have observed a consistent decrease in the area of electrospray plumes as the organic content of the sprayed solvent is increased (data not shown). This is likely because the decrease in ion current with increasing organic content decreases coulombic repulsions. A narrower spray plume in general will mean a higher ion transmission efficiency, which only adds to the reasons researchers have traditionally seen better signal-to-noise with at least some organic content in the mobile phase [10, 16, 17, 49].

Improving Ion Transmission Using an Electrostatic Lens

Results from the ESI profiler led us to believe we could expect roughly 3-fold increase in ion transmission effi-

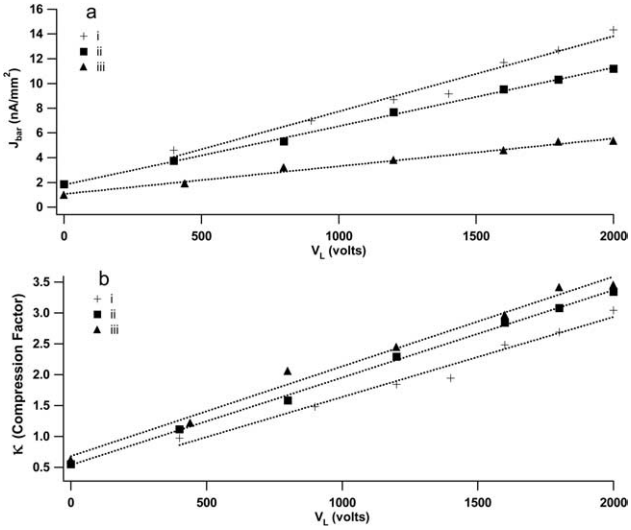

Figure 7. Effectiveness of lens with hemispherical interior under different solvent conditions. F ~ 15 nL/min. (**a**) Average current density versus lens voltage. (**b**) Compression Factor versus lens voltage. (i) 10% acetonitrile in 0.1% formic acid. (ii) 40% acetonitrile in 0.1% formic acid. (iii) 80% acetonitrile in 0.1% formic acid.

ciency by using a hemispherical electrostatic lens to focus a nano-ESI plume. In order to experimentally verify this hypothesis, a series of experiments were performed using a single-quadrupole mass spectrometer (Micromass ZQ). The current at a small mesh electrode placed in the first vacuum region was monitored and compared to the total ESI current to determine the ion transmission into the first orifice (see Experimental section). In a series of infusion experiments performed, total spray currents varied widely depending on the flow rate, spray voltage, mobile phase composition, and needle position used, but followed the trends reported in the literature [4–6, 9, 12, 17]. However, in our ion transmission measurements using nano-ESI, we were surprised to find much higher transmission efficiencies than previously reported.

Figure 8 is a plot of transmission efficiency into the first orifice as a function of distance between the needle and the acceptance orifice, for the nano-ESI of 50/50 water/acetonitrile with 0.1% formic acid and 950 nM neurotensin at 30 nL/min. Transmission efficiency was calculated simply as the ratio of the current at the mesh electrode to the total ESI current. A leakage current of 0.7 nA was subtracted from the measured current at the mesh. Figure 8 indicates that 68% ion transmission was obtained for the closest needle-to-orifice position (15.3 nA out of 23.2 nA total current). However, when the mesh was removed and ion intensity was recorded for the 559 *m/z* ion of neurotensin, the optimal ion count was observed when the distance was roughly 2 to 2.5 mm, where ion transmission was about 40%. The ESI mechanism needs a certain amount of time at atmospheric pressure to create gas-phase ions, as has been indicated by inefficient ionization when ESI was performed directly into vacuum [50]. It is possible that the distance of roughly 2.5 mm in this experiment provided the optimum balance between efficient ionization and ion transfer, assuming these are the two dominant mechanisms in place.

The ion transmission efficiencies in our experiments represent a large departure from the literature, where 99% or more of the ion current is reported lost prior to the first vacuum region [10, 16–18]. However, previous reports of direct ion transmission have been run under conditions where flow rates are near 1 μL/min, which is more than an order of magnitude higher than our experimental flow rate. It appears that the faster desolvation and lower space-charge of nanoliter-per-minute flow rates allow the gas dynamics of an orifice to be much more effective at ion conductance. This data also suggests that future efforts undertaken to improve on ion transmission for nano-ESI must recognize that improving upon a starting condition of 40% transmission efficiency may be much more difficult than if the starting condition were 1% transmission.

In order to determine if an electrostatic lens could further improve ion transmission, the hemispherical lens was positioned in a manner similar to in Figure 2, with the spray needle 4mm from the acceptance orifice of the ZQ mass spectrometer. The starting ion transmission into the first orifice, with the hemispherical lens at 0 V, was roughly 24%. This was boosted to about 45% transmission by using a lens voltage of 560 V. During this experiment the signal was also monitored for the 559 *m/z* ion of neurotensin, even though only a small fraction of the ions were reaching the mass analyzer (the majority was being collected by the mesh electrode). With the lens off, the average signal over a 0.4 min collection period measured 2.84×10^5 counts. With the lens on, the signal was 4.99×10^5 counts, corresponding to an increase of roughly 76%.

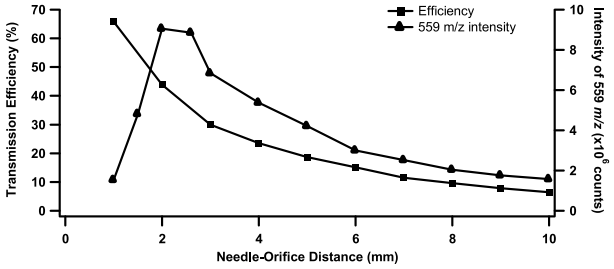

Figure 8. Ion transmission efficiency and neurotensin $(M+3H)^{3+}$ ion intensity as a function of needle to orifice distance for nano-ESI. Experiment was run with a flow rate of 30 nL/min of 50/50 water/acetonitrile with 0.1% formic acid and 950 nM neurotensin, using an FS360-20-5-D spray needle. Spray voltage was increased from 900 V at 1 mm to 1.30 kV at 10 mm to maintain roughly constant total spray current. Even though ion transmission is highest at 1 mm (68%), the optimal mass spec signal for the neurotensin peak occurred between 2 and 2.5 mm, where transmission is 35 to 45%.

Percent Coverage of a Protein Digest

In order to evaluate the real-world utility of the apparent signal doubling that was observed with the hemispherical electrostatic lens, a LC-MS experiment was performed as discussed in the experimental section. Each run used a 120-min gradient elution from 5 to 50% acetonitrile in 0.1% formic acid, and the average peak width was roughly 15 s. Figure 9 shows the results of this experiment, plotted as percent coverage versus amount injected. Although the lens helped to pick up a few peptides in most experiments in the middle injection ranges (1–10 fmol injected), the overall improvement in percent coverage is nominal, if any.

Conclusions

We find that electrostatic lenses work to focus nano-ESI plumes at atmospheric pressure, but in our experience do not enhance MS signals enough to significantly benefit the everyday user. Experiments described herein show that nano-ESI-MS performs at higher ion transmission efficiency than previously expected; there is less room for improvement in signal-to-noise by trying to increase ion transmission into the first orifice in ESI-MS. It is also possible that ionization efficiency

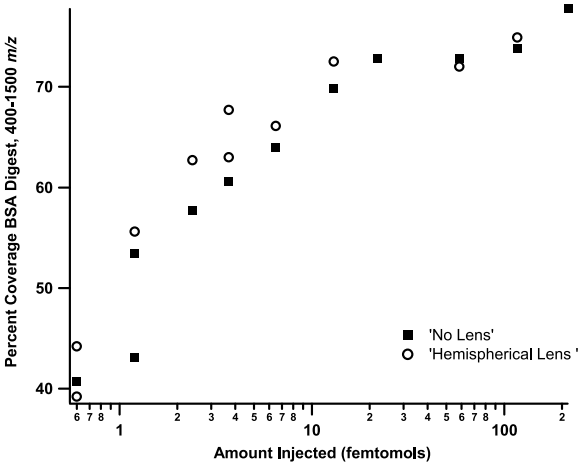

Figure 9. Percent coverage of bovine serum albumin tryptic digest versus quantity injected, from an LC-MS experiment using a 50 cm × 30 μm capillary column packed with 3 um Atlantis C18 particles. Gradient: 5 to 50% acetonitrile with 0.1% formic acid over 120 mins. F = 15 nL/min; V_s = 1400 V; hemispherical lens runs were done with V_L = 600 V.

suffers as a result of using electrostatic lenses to compress the ESI plume. As droplets are emitted from the Taylor cone, coulombic repulsion between ions typically assists the desolvation-coulombic explosion process which ultimately leads to gas-phase ions [2–6]. If the electrostatic field from the ion lens is effective at fighting space-charge to increase ion density in the center of the plume, as we have shown, then it may also decrease the rate of desolvation. In this case, use of electrostatic ion lenses around an electrospray needle would lead to more efficient ion transfer, but less efficient gas-phase ionization, with no resultant net gain in signal.

The two major weaknesses of the ESI profiler are its inability to function properly at high liquid volumetric flow rates and that it ignores gas dynamic effects on ion transmission into mass spectrometers. At flow rates greater than about 500 nL/min, droplets form on the ground plane during the collection of a profile, even at distances of 4 cm or more. However, we feel that because of the excess space-charge present in ESI at high flow rates, focusing with electrostatics may not be a viable option in that regime. Furthermore, nano-ESI offers superior ionization efficiency and sensitivity as previously discussed, so concentrating on improving ion transmission for nano-ESI is not seen as a hindrance. Although only electrostatic lenses were tested in the experiments reported here, the ESI profiler would likely perform as well in measuring effects of electrodynamic, gas dynamic, or other focusing methods on nano-ESI.

Our data show that 40% ion transmission into the first vacuum region of a mass spectrometer is probably not uncommon for what have become typical nano-ESI conditions. The increase in signal observed with decreasing flow rate has previously been almost totally ascribed to increases in ionization efficiency [9–12, 51]. Our findings indicate that the increase in signal with nano-ESI is likely due to benefits both in ionization efficiency and ion transmission efficiency.

Acknowledgments

The authors sincerely thank Waters Corporation for financial support of this research and for providing the ZQ mass spectrometer used in the ion transmission studies. They also give special thanks to Dr. Keith Fadgen.

References

1. Yamashita, M.; Fenn, J. B. Electrospray Ion Source: Another Variation on the Free-Jet Theme. *J. Phys. Chem.* **1984,** *88*, 4451–4459.
2. Kebarle, P.; Tang, L. From Ions in Solution to Ions in the Gas Phase. *Anal. Chem.* **1993,** *65*, 972A–986A.
3. Cole, R. B. Some Tenets Pertaining to Electrospray Ionization Mass Spectrometry. *J. Mass. Spectrom.* **2000,** *35*, 763–772.
4. Cech, N. B.; Enke, C. G. Practical Implications of Some Recent Studies in Electrospray Ionization Fundamentals. *Mass Spectrom. Rev.* **2001,** *20*, 362–387.
5. Kebarle, P. A Brief Overview of the Present Status of the Mechanisms Involved in Electrospray Mass Spectrometry. *J. Mass. Spectrom.* **2000,** *35*, 804–817.
6. Bruins, A. P. Mechanistic Aspects of Electrospray Ionization. *J. Chromatogr. A* **1998,** *794*, 345–357.
7. Tang, L.; Kebarle, P. Effect of the Conductivity of the Electrosprayed Solution on the Electrospray CurrentFactors Determining Analyte Sensitivity in Electrospray Mass Spectrometry. *Anal. Chem.* **1991,** *63*, 2709–2715.
8. Wahl, J. H.; Goodlet, D. R.; Udseth, H. R.; Smith, R. D. Attomole Level Capillary Electrophoresis-Mass Spectrometric Protein Analysis Using 5-um-i.d. Capillaries. *Anal. Chem.* **1992,** *64*, 3194–3196.
9. Mann, M.; Wilm, M. Electrospray and Taylor-Cone Theory, Dole's Beam of Macromolecules at Last? *Int. J. Mass Spectrom. Ion Processes* **1994,** *136*, 167–180.
10. Wilm, M.; Mann, M. Analytical Properties of the Nanoelectrospray Ion Source. *Anal. Chem.* **1996,** *68*, 1–8.
11. Feng, B.; Smith, R. D. A Simple Nanoelectrospray Arrangement with Controllable Flowrate for Mass Analysis of Submicroliter Protein Samples. *J. Am. Soc. Mass Spectrom.* **2000,** *11*, 94–99.
12. Schmidt, A.; Karas, M.; Dulcks, T. Effect of Different Solution Flow Rates on Analyte Ion Signals in Nano-ESI MS, orWhen does ESI Turn into Nano-ESI? *J. Am. Soc. Mass Spectrom.* **2003,** *14*, 492–500.
13. Busman, M.; Sunner, J.; Vogel, C. R. Space-Charge-Dominated Mass Spectrometry Ion SourcesModeling and Sensitivity. *J. Am. Soc. Mass Spectrom.* **1991,** *2*, 1–10.
14. Smith, R. D.; Olivares, J. A.; Nguyen, N. T.; Udseth, H. R. Capillary Zone Electrophoresis-Mass Spectrometry Using an Electrospray Ionization Interface. *Anal. Chem.* **1988,** *60*, 436–441.
15. Olivares, J. A.; Nguyen, N. T.; R.Yonker, C.; Smith, R. D. On-Line Mass Spectrometric Detection for Capillary Zone Electrophoresis. *Anal. Chem.* **1987,** *59*, 1230–1232.
16. Smith, R. D.; Loo, L. A.; Edmonds, C. G.; Barinaga, C. J.; Udseth, H. R. New Developments in Biochemical Mass SpectrometryElectrospray Ionization. *Anal. Chem.* **1990,** *62*, 882–899.
17. Zook, D. R.; Bruins, A. P. On Cluster Ions, Ion Transmission, and Linear Dynamic Range Limitations in Electrospray (Ion-

spray) Mass Spectrometry. *Int. J. Mass Spectrom. Ion Processes* **1997,** *162*, 129–147.
18. Shaffer, S. A.; Tang, K.; Anderson, G. A.; Prior, D. C.; Udseth, H. R.; Smith, R. D. A Novel Ion Funnel for Focusing Ions at Elevated Pressure Using Electrospray Ionization Mass Spectrometry. *Rapid Commun. Mass Spectrom.* **1997,** *11*, 1813–1817.
19. Kim, T.; Udseth, H. R.; Smith, R. D. Improved Ion Transmission from Atmospheric Pressure to High Vacuum Using a Multicapillary Inlet and Electrodynamic Ion Funnel Interface. *Anal. Chem.* **2000,** *72*, 5014–5019.
20. Bruins, A. P. Mass Spectrometry with Ion Sources Acting at Atmospheric Pressure. *Mass Spectrom. Rev.* **1991,** *10*, 53–77.
21. Bahr, R.; Gerlich, D.; Teloy, E. Ring Electrode Ion Guide. E. Verh. Dtsch. Phys. Ges.(IV) 1969, 4, 343.
22. Shaffer, S. A.; Prior, D. C.; Anderson, G. A.; Udseth, H. R.; Smith, R. D. An Ion Funnel Interface for Improved Ion Focusing and Sensitivity Using Electrospray Ionization Mass Spectrometry. *Anal. Chem.* **1998,** *70*, 4111–4119.
23. Shaffer, S. A.; Tolmachev, A.; Prior, D. C.; Anderson, G. A.; Udseth, H. R. Characterization of an Improved Electrodynamic Ion Funnel Interface for Electrospray Ionization Mass Spectrometry. *Anal. Chem.* **1999,** *71*, 2957–2964.
24. Belov, M. E.; Gorshkov, M. V.; Udseth, H. R.; Anderson, G. A.; Tolmachev, A.; Prior, D. C.; Harkewicz, R.; Smith, R. D. Initial Implementation of an Electrodynamic Ion Funnel With Fourier Transform Ion Cyclotron Resonance Mass Spectrometry. *J. Am. Soc. Mass Spectrom.* **2000,** *11*, 19–23.
25. Lynn, E. T.; Chung, M.-C.; Han, C.-C. Characterizing the Transmission Properties of an Ion Funnel. *Rapid Commun. Mass Spectrom.* **2000,** *14*, 2129–2134.
26. Tolmachev, A.; Kim, T.; Udseth, H. R.; Smith, R. D.; Bailey, T. H.; Futrell, J. H. Simulation-Based Optimization of the Electrodynamic Ion Funnel for High Sensitivity Electrospray Ionization Mass Spectrometry. *Int. J. Mass Spectrom.* **2000,** *203*, 31–47.
27. Kim, T.; Tang, K.; Udseth, H. R.; Smith, R. D. A Multicapillary Inlet Jet Disruption Electrodynamic Ion Funnel Interface for Improved Sensitivity Using Atmospheric Pressure Ion Sources. *Anal. Chem.* **2001,** *73*, 4162–4170.
28. Tang, K.; Tolmachev, A.; Nikolaev, E.; Zhang, R.; Belov, M. E.; Udseth, H. R.; Smith, R. D. Independent Control of Ion Transmission in a Jet Disrupter Dual-Channel Ion Funnel Electrospray Ionization MS Interface. *Anal. Chem.* **2002,** *74*, 5431–5437.
29. Zhou, L.; Yue, B.; Dearden, D. V.; Lee, E. D.; Rockwood, A. L.; Lee, M. L. Incorporation of a Venturi Device in Electrospray Ionization. *Anal. Chem.* **2003,** *75*, 5978–5983.
30. Potjewyd, J. *Focusing of Ions in Atmospheric Pressure Gases Using Electrostatic Fields*; Ph.D. Thesis, University of Toronto, 1983.
31. Sheehan, E. W.; Willoughby, R. C. Apparatus and Method for Focusing Ions and Charged Particles at Atmospheric Pressure; U.S. Patent Application 20020011560, 2002.
32. Jochen, F. Method and Device for the Introduction of Ions into the Gas Stream of an Aperture to a Mass Spectrometer; Bruker-Franzen Analytik GmbH: U.S. Patent 5,747,799, 1996.
33. Gulcicek,, E. E., Whitehouse,, C. M. Ion Focusing Lensing System for a Mass Spectrometer Interfaced to an Atmospheric Pressure Ion Source; U.S. Patent 5,432,343, 1995.
34. Schneider, B. B.; Douglas, D. J.; Chen, D. D. Y. An Atmospheric Pressure Ion Lens to Improve Electrospray Ionization at Low Flow Rates. *Rapid Commun. Mass Spectrom.* **2001,** *15*, 2168–2175.
35. Beavis, R. C.; Ens, W.; Main, D. E.; Standing, K. G. Off-Line Coupling to a Microbore High-Performance Liquid Chromatograph of a Secondary Ion Time-of-Flight Mass Spectrometer. *Anal. Chem.* **1990,** *62*, 1259–1264.
36. Beavis, R. C.; Bolbach, G.; Ens, W.; Main, D. E.; Schueler, B.; Standing, K. G.; Automated Dry Fraction Collection For Microbore High-Performance Liquid Chromatography-Mass Spectrometry. *J. Chromatogr. A* **1986,** *359*, 489–497.
37. Zhou, S.; Edwards, A. G.; Cook, K. D.; Van Berkel, G. J. Investigation of the Electrospray Plume by Laser-Induced Fluorescence Spectroscopy. *Anal. Chem.* **1999,** *71*, 769–776.
38. Zhou, S.; Prebyl, B. S.; Cook, K. D. Profiling pH Changes in the Electrospray Plume. *Anal. Chem.* **2002,** *74*, 4885–4888.
39. MacNair, J. E.; Lewis, K. C.; Jorgenson, J. W. Ultrahigh-Pressure Reversed-Phase Liquid Chromatography in Packed Capillary Columns. *Anal. Chem.* **1997,** *69*, 983–989.
40. Jones, A. R.; Thong, K. C. The Production of Charged Monodisperse Fuel Droplets by Electrical Dispersion. *J. Phys. D Appl. Phys.* **1971,** *4*, 1159–1168.
41. Smith, D. P. H. The Electrohydrodynamic Atomization of Liquids. *IEEE Trans. Ind. App.* **1986,** *IA-22*, 527–535.
42. Juraschek, R.; Röllgen, F. W. Pulsation Phenomena During Electrospray Ionization. *Int. J. Mass Spectrom.* **1998,** *177*, 1–15.
43. Ikonomou, M. G.; Blades, A. T.; Kebarle, P. Electrospray-Ion Spray: A Comparison of Mechanisms and Performance. *Anal. Chem.* **1991,** *63*, 1989–1998.
44. Blades, A. T.; Ikonomou, M. G.; Kebarle, P. Mechanism of Electrospray Mass Spectrometry: Electrospray as an Electrolysis Cell. *Anal. Chem.* **1991,** *63*, 2109–2114.
45. Smith, J. N.; Flagan, R. C.; Beauchamp, J. L. Droplet Evaporation and Discharge Dynamics in Electrospray Ionization. *J. Phys. Chem. A* **2002,** *106*, 9957–9967.
46. Loscertales, I. G.; de la Mora, J. F. Experiments on the Kinetics of Field Evaporation of Small Ions from Droplets. *J. Chem. Phys.* **1995,** *103*, 5041–5060.
47. Enke, C. G. A Predictive Model for Matrix and Analyte Effects in Electrospray Ionization of Singly-Charged Ionic Analytes. *Anal. Chem.* **1997,** *69*, 4885–4893.
48. Cech, N. B.; Enke, C. G. Relating Electrospray Ionization Response to Nonpolar Character of Small Peptides. *Anal. Chem.* **2000,** *72*, 2717–2723.
49. Geromanos, S.; Freckleton, G.; Tempst, P. Tuning of an Electrospray Ionization Source for Maximum Peptide-Ion Transmission into a Mass Spectrometer. *Anal. Chem.* **2000,** *72*, 777–790.
50. Dohmeier, D. M. *Open Tubular Liquid Chromatography: Studies in Column Efficiency and Detection*; Ph.D. Thesis, University of North Carolina at Chapel Hill, 1991.
51. Juraschek, R.; Dulcks, T.; Karas, M. Nanoelectrospray—More Than Just a Minimized-Flow Electrospray Ionization Source. *J. Am. Soc. Mass Spectrom.* **1999,** *10*, 300–308.